Journal of Hazardous Materials 401 (2021) 123327

Contents lists available at ScienceDirect

Journal of Hazardous Materials

journal homepage: www.elsevier.com/locate/jhazmat

Arsenic removal from natural groundwater using 'green rust': Solid phase stability and contaminant fate

Jeffrey Paulo H. Perez[a,b,*], Adrian Alexander Schiefler[c,d], Sandra Navaz Rubio[a,b], Markus Reischer[c,e], Niels Døssing Overheu[d], Liane G. Benning[a,b], Dominique J. Tobler[c]

[a] GFZ German Research Center for Geosciences, Telegrafenberg, 14473 Potsdam, Germany
[b] Department of Earth Sciences, Freie Universität Berlin, Malteserstr. 74-100, 12249 Berlin, Germany
[c] Nano-Science Center, Department of Chemistry, University of Copenhagen, Universitetsparken 5, 2100 Copenhagen, Denmark
[d] Capital Region of Denmark, Kongens Vænge 2, 3400 Hillerød, Denmark
[e] NIRAS A/S, Sortemosevej 19, 3450 Allerød, Denmark

GRAPHICAL ABSTRACT

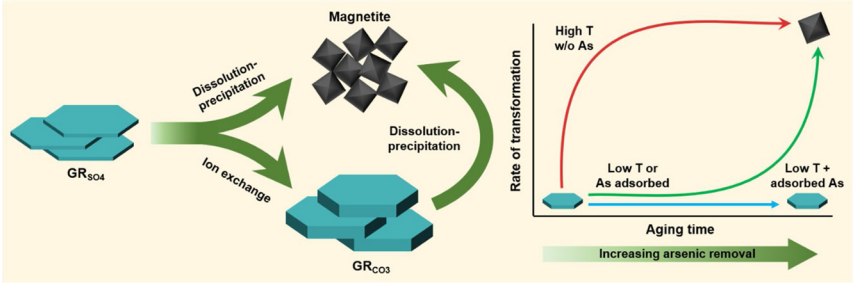

ARTICLE INFO

Editor: T Meiping

Keywords:
Adsorption
Aging effects
Groundwater remediation
Iron (oxyhydr)oxides
Mineral stability

ABSTRACT

Arsenic (As) contamination in groundwater remains a pressing global challenge. In this study, we evaluated the potential of green rust (GR), a redox-active iron phase frequently occurring in anoxic environments, to treat As contamination at a former wood preservation site. We performed long-term batch experiments by exposing synthetic GR sulfate (GR_{SO4}) to As-free and As-spiked (6 mg L^{-1}) natural groundwater at both 25 and 4 °C. At 25 °C, GR_{SO4} was metastable in As-free groundwater and transformed to GR_{CO3}, and then fully to magnetite within 120 days; however, GR_{SO4} stability increased 7-fold by lowering the temperature to 4 °C, and 8-fold by adding As to the groundwater at 25 °C. Highest GR_{SO4} stability was observed when As was added to the groundwater at 4 °C. This stabilizing effect is explained by GR solubility being lowered by adsorbed As and/or lower temperatures, inhibiting partial GR dissolution required for transformation to GR_{CO3}, and ultimately to magnetite. Despite these mineral transformations, all added As was removed from As-spiked samples within 120 days at 25 °C, while uptake was 2 times slower at 4 °C. Overall, we have successfully documented that GR is an important mineral substrate for As immobilization in anoxic subsurface environments.

1. Introduction

From 1930s to 1990s, chromated copper arsenate (CCA) was widely used as a wood preservative, replacing most oil-based preservatives (e.g., creosote) and pentachlorophenol (Humphrey, 2002). The extensive use of CCA in the wood preservation industry resulted in the

* Corresponding author at: GFZ German Research Center for Geosciences, Telegrafenberg, 14473 Potsdam, Germany.
E-mail address: jpperez@gfz-potsdam.de (J.P.H. Perez).

https://doi.org/10.1016/j.jhazmat.2020.123327
Received 21 April 2020; Received in revised form 13 June 2020; Accepted 24 June 2020
Available online 27 June 2020

uncontrolled release of these metal(loids) into underlying soils and groundwater (Nielsen et al., 2016, 2011), and nearby surface waters (Bhattacharya et al., 2002). Arsenic (As), which makes up ~30 % wt. of CCA formulations, is highly mobile compared to copper (Cu) and chromate (Cr), and can penetrate deep into the soil layers (Hingston et al., 2001; Stilwell and Gorny, 1997; Zagury et al., 2003). In CCA-contaminated soils and groundwater, As is commonly present as the inorganic species arsenite [As(III)] and arsenate [As(V)]. Both these species persist in oxic and anoxic conditions due to their relatively slow redox transformation kinetics (Masscheleyn et al., 1991; Zagury et al., 2008).

A way to mitigate As toxicity and mobility in contaminated soils and groundwater is the use of natural attenuation processes (Reisinger et al., 2005). This primarily involves As sorption to naturally occurring metal (oxyhydr)oxide phases (i.e., Fe, Al, Mn) (Wang and Mulligan, 2006), or the precipitation of secondary As-bearing phases (Raghav et al., 2013). Specifically, iron (oxyhydr)oxides, which are ubiquitous in nature, can effectively remove As either by adsorption or co-precipitation. Previous studies have shown that iron (oxyhydr)oxides can reduce contamination levels at As-contaminated field sites to background concentrations (Asta et al., 2010; Carlson et al., 2002; Fukushi et al., 2003; Maillot et al., 2013).

Many contaminated groundwaters rapidly become anoxic in subsurface environments. In such cases, it is mostly the ubiquitous redox-active iron phases that are particularly important substrates for As sequestration. In anoxic non-sulfidogenic settings, green rust (GR), a mixed-valent iron layered double hydroxide, is a common Fe-bearing phase (Linke and Gislason, 2018). GR phases consist of positively-charged Fe^{II}-Fe^{III} hydroxide sheets that alternate with negatively-charged hydrated interlayers with anions (e.g., Cl^-, CO_3^{2-}, SO_4^{2-}) (Usman et al., 2018), and occasional monovalent cations (Christiansen et al., 2014). They are increasingly observed in natural settings, despite the fact that sampling and handling of GR is difficult due to its high oxygen sensitivity. For example, GR has been identified in anoxic environments such as gley soils (Abdelmoula et al., 1998; Trolard et al., 1997), groundwater (Christiansen et al., 2009a), ferruginous (Fe^{2+}-rich) lakes (Koeksoy et al., 2019; Vuillemin et al., 2019; Zegeye et al., 2012), mofette sites (Rennert et al., 2012) or mine drainage sites (Bearcock et al., 2006; Johnson et al., 2014). Importantly, naturally occurring GR particles have been reported to sorb arsenic (Root et al., 2007), as well as other heavy metals (e.g., Cu, Ni, Pb, Zn) (Dore et al., 2020; Johnson et al., 2014, 2015) in contaminated environments. Although these studies have successfully shown that GR can immobilize these metals, little to none is known about the fate of these metal-bearing GR phases upon aging in subsurface environments. This is despite the fact that GR phases, like many other Fe phases that have high metal sorption capacities (e.g., ferrihydrite, schwertmannite, jarosite), are metastable and will eventually transform, which could result in the re-release of any immobilized metals.

In this study, we evaluated the potential of GR phases as substrates for the natural attenuation of As in a former CCA treatment site in Denmark. At this site, the majority of the contamination is located within the top 0.5 m soil layer, consisting of Cu, Cr (each ~100 mg kg^{-1}) and very high As concentrations (~2000 mg kg^{-1}) (Aktor and Nielsen, 2011; Nielsen et al., 2011). Due to its high mobility, As is, however, also present in the underlying shallow aquifer (ca. 100–600 µg L^{-1}, depth ~5 m) and to some extent in the deeper aquifer (0.1 to 0.5 µg L^{-1}, depth ~20 m). According to a previous technical report by the Danish Environmental Protection Agency (EPA) (Aktor and Nielsen, 2011), significant As leakage into the deep aquifer is inhibited by the presence of Fe (oxyhydr)oxides in the upper soil layers, but no further information was given. Based on initial thermodynamic modelling of the monitoring data, we predicted that GR sulfate (GR_{SO4}) is a dominant iron phase in the deeper, anoxic zone at this site. Because it is highly reactive, GR could therefore play a key role in prohibiting As from leaking into the deeper aquifer. However, how stable any As-bearing GR is upon prolonged aging in the groundwater is unknown, and the question about the ultimate fate of As in the environment in case that GR transformations occur, is also unsolved.

To investigate this, we collected groundwater samples from different soil depths at this former CCA treatment site, characterized their water chemistry and performed thermodynamic modelling to reaffirm the hypothesized presence of GR in the deeper, anoxic zones. Next, we set up long-term aging experiments (up to 1 year) where synthetic GR sulfate (GR_{SO4}) was exposed to the collected, anoxic groundwater at two different temperatures. In addition, we also spiked the collected groundwater with higher As concentrations (~6 mg L^{-1}) and exposed GR to it at two temperatures to test the effects on the stability of As-bearing GR. Our results provide new insights into the potential role of GR for controlling the mobility and toxicity of As in contaminated subsurface environments, while also highlighting the geochemical parameters that control GR long-term stability in subsurface environments.

2. Methods

2.1. Site description

The investigated Collstrop site in the town of Hillerød in Denmark (55°57′ N, 12°21′ E) (Fig. 1) was a former CCA treatment facility that operated from 1936 to 1976. Since December 2015, the Collstrop site is managed by the Capital Region of Denmark and is currently being used to test remediation technologies for heavy metals. During the operation of the CCA treatment facility, the top soil became heavily contaminated with Cu, Cr (each ~100 mg kg^{-1}) and As (~2000 mg kg^{-1}) through spills from tanks and by drippings from treated timber (Aktor and Nielsen, 2011; Nielsen et al., 2011). The soil at the site consists of 1–5 meters of alternating sand and clay layers from glacial deposits, which host a shallow groundwater aquifer (ternary aquifer). The water table is about 3 m below the surface. Underneath the shallow aquifer is a clay till layer of varied thickness (4–19 m thick). This is followed by the deeper groundwater aquifer (secondary aquifer), which is composed of a layer of relatively homogenous alluvial sand (20–40 m thick). A connection between the ternary and secondary aquifer has not been confirmed yet, but the average infiltration rates into the secondary aquifers at this site was estimated to be 35–135 mm y^{-1} (Aktor and Nielsen, 2011). A lower clay till layer (13–40 m) separates the secondary aquifer from the primary aquifer. The primary aquifer is composed of alluvial sands and limestone below the sand.

2.2. Groundwater sampling and analyses

Water samples were collected from Eks.P1 (surface ditch, oxic), well 129 (shallow aquifer, oxic) and well MD2 (secondary aquifer, anoxic, Fig. S1) on February 2018 using an electric submersible pump. For groundwater extraction from wells 129 and MD2, the wells were first pumped until field parameters (i.e., pH, oxygen reduction potential (ORP), electrical conductivity (EC), dissolved oxygen (DO), temperature) stabilized (Table S2). ORP, EC and DO and pH were measured using a WTW Multi 3420 and WTW Multi 3430 handheld meter. The groundwater samples were collected in acid-cleaned (0.3 M HNO_3) airtight 1-L glass bottles (Duran®) and quickly (within ~1 h) transported to the laboratory for processing. Once in the laboratory, the collected groundwater samples were placed inside an anaerobic chamber (97 % N_2, 3 % H_2, Coy Laboratory Products, Inc.) and immediately filtered through 0.2-µm polyethersulfone (PES) membrane filters to avoid equilibration with the chamber atmosphere. An aliquot of the filtrate was transferred to acid-cleaned 13-mL polypropylene (PP) vials and acidified with concentrated HNO_3 (Honeywell TRaceSELECT™ Ultra) for inductively coupled plasma mass spectrometry (ICP-MS) analyses. Another aliquot was directly filtered into acid-cleaned 20-mL crimp top glass vials (leaving no headspace), crimp capped and

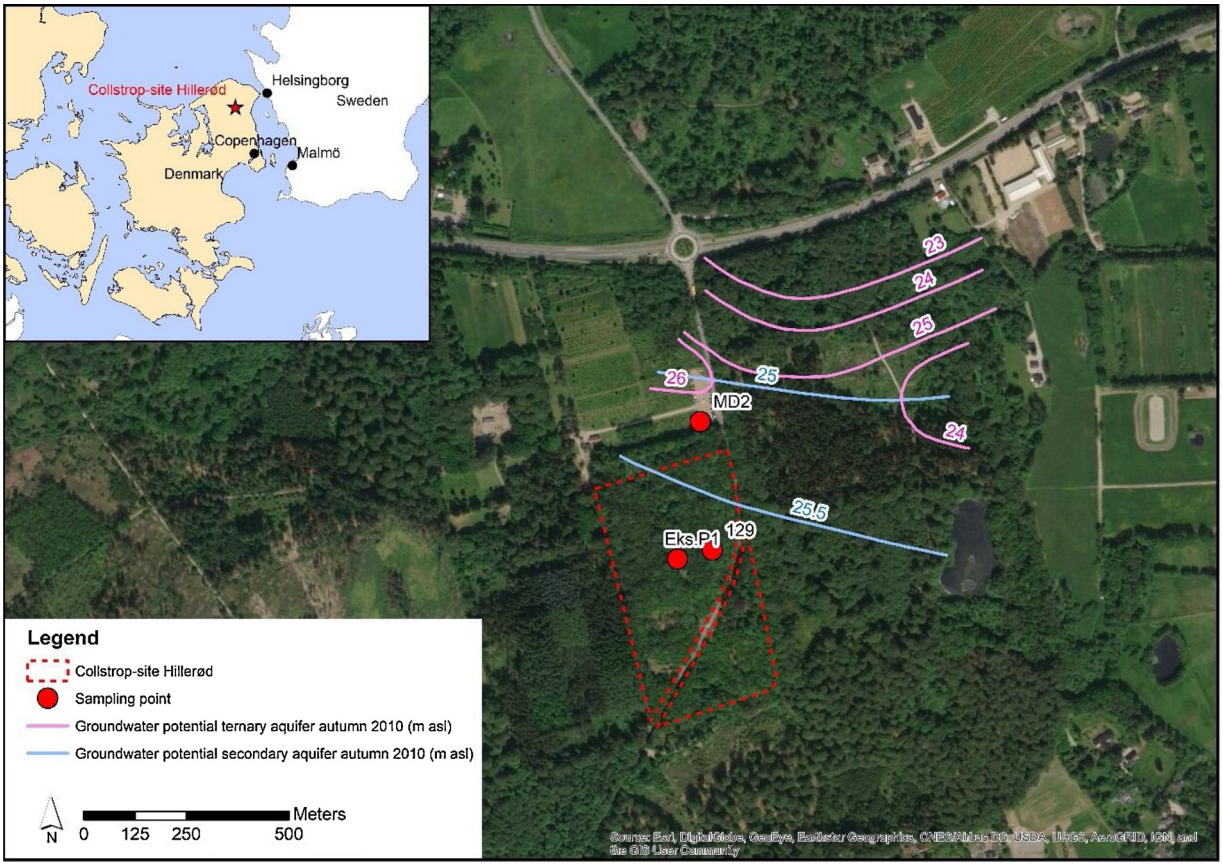

Fig. 1. Location and distribution of the sampling sites (red dots) at the studied CCA treatment site in Hillerød, Denmark. The general flow directions of the ternary (magenta lines) and secondary (blue lines) aquifer are also shown (Aktor and Nielsen, 2011).

wrapped in aluminum foil for ion chromatography (IC) analyses. All samples were stored at 4 °C until analysis.

2.3. Synthesis of green rust sulfate (GR_{SO4})

All used laboratory glass- and plasticwares were cleaned by soaking them in 0.3 M HNO_3 for at least 24 h, followed by thorough rinsing with deionized water (~18.2 MΩ cm). All used reagents were of analytical grade from Sigma-Aldrich and Acros Organics. Stock solutions for GR_{SO4} synthesis were prepared inside the anaerobic chamber using deoxygenated deionized water obtained by bubbling it with O_2- and CO_2-free nitrogen for at least 4 h.

GR_{SO4} was synthesized by aqueous Fe(II) oxidation at constant pH inside the anaerobic chamber (Mangayayam et al., 2018). In a PFA vessel, 50 mM $FeSO_4{\cdot}7H_2O$ was oxidized by bubbling CO_2-free air at a constant rate of 5.0 ± 0.5 mL min^{-1} using a peristaltic pump while maintaining the pH at ~7 by titration of 1 M NaOH. Oxidation and titration were stopped immediately after reaching an $[Fe]_{total}/[OH^-]$ ratio of ~4.55. The supernatant of the freshly precipitated GR_{SO4} was removed and the remaining slurry was washed with O_2-free Milli-Q water to remove excess solutes (Perez et al., 2020). After washing, the supernatant was removed to obtain a thick slurry of GR_{SO4}. The amount of GR solids (mM Fe_{GR}) was determined based on the difference between the total Fe concentration, $[Fe_{susp}]$, of an aliquot of the slurry dissolved in 0.3 M HNO_3 and the dissolved Fe concentration, $[Fe_{(aq)}]$, in the supernatant after filtration through a 0.2-µm syringe filter. The iron concentrations were analyzed by atomic absorption spectroscopy (AAS). The produced GR_{SO4} slurries (~152 mM Fe_{GR}) were used for aging experiments on the day of synthesis.

2.4. GR_{SO4} aging in deep aquifer groundwater

In 100-mL crimp cap glass bottles, an aliquot of the GR_{SO4} slurry was diluted to 90 mL using the as-collected (hereafter referred to as As-free) groundwater from well MD2 (deep aquifer) to achieve an $[Fe_{GR}]$ of ~12.5 mM. In another set-up, the groundwater was spiked with 6 mg L^{-1} As (~80 µM), consisting of equimolar amounts of As(III) and As (V), to simulate their frequent co-occurrence in anoxic environments (Masscheleyn et al., 1991; Zagury et al., 2008). The added As concentration is ~2 orders of magnitude above the background concentration in the as-collected groundwater sample. The effect of water depth was examined by aging the samples at 25 °C inside the anaerobic chamber, and at 4 °C inside a refrigerator. The initial groundwater pH was ~7.5 and only marginally varied during aging (± 0.3 pH units). All experiments were done in triplicate. Aliquots of the GR suspension were collected after 1, 7, 15, 30, 60, 120 days, and 1 year. A portion of the collected sample was filtered (0.2-µm syringe filters), and the filtrate was acidified with HNO_3 and stored in acid-cleaned vials at 4 °C. Major aqueous elemental concentrations were determined by inductively coupled plasma optical emission spectroscopy (ICP-OES Varian 720ES) as described in our previous work (Perez et al., 2019a), and detection limits and analytical uncertainties can be found in the Supplementary Information (Table S1). The rest of the collected experimental aliquots were used to obtain solids for characterization. For this, a 10 mL suspension aliquot was transferred into 20-mL crimp vials, crimp capped and centrifuged outside of the anaerobic chamber. Afterwards, the solids were separated inside the chamber and prepared for X-ray powder diffraction (XRD) and scanning electron microscopy (SEM) imaging.

2.5. Analytical methods, mineral characterization and thermodynamic modelling

Major, minor and trace element concentrations in the as-collected groundwater samples were measured by a quadrupole inductively coupled plasma mass spectrometry (ICP-MS, Thermo Fisher Scientific iCAP-Qc). Aqueous Fe^{2+} concentrations were analyzed spectrophotometrically using the ferrozine method (Viollier et al., 2000). Dissolved inorganic and organic anions in the as-collected groundwater samples were analyzed by suppressed IC system (Sykam Chromatographie) using a SeQuant SAMS anion IC suppressor (EMD Millipore), an S5200 sample injector, a 3.0 × 250 mm lithocholic acid 14 column and an S3115 conductivity detector. The eluent was 5 mM Na_2CO_3 with 20 mg L^{-1} 4-hydroxybenzonitrile and 0.2 % methanol. The flow rate was set to 1 mL min^{-1} and the column oven temperature to 50 °C.

XRD patterns were recorded on a Bruker D-8 Discover powder diffractometer equipped with a Lynxeye 1-D detector operating at 40 kV and 40 mA using Cu Kα radiation (λ = 1.5406 Å) with a 0.017° step, a 2.5 s per step scan length, and 2θ from 5° to 70°. Samples for XRD analysis were loaded onto a silicon wafer and the sample holder was sealed using a X-ray transparent dome (Bruker Dome, Polytron) with a low diffusion rate to minimize sample oxidation. Phase quantification was done via Rietveld refinement of the XRD patterns using the software GSASII (Toby and Von Dreele, 2013). The high background produced by the dome was corrected by subtracting the XRD pattern of the empty sample holder from the sample XRD, and by applying a Savitzky-Golay smoothing filter. In addition, the background was determined separately from the Rietveld refinement using a Chebyshev polynomial. The instrumental parameters were refined from a corundum standard.

Particle morphologies and sizes of the aged solids were characterized by SEM (Quanta 3D, 10 kV). Samples for SEM imaging were prepared inside the anaerobic chamber by suspending an aliquot of a solid sample in ethanol and drop-casting the suspension onto SEM stubs.

Thermodynamic calculations were carried out using The Geochemist's Workbench® (Bethke, 2010) with the MINTEQ database and the chemical compositions of the analyzed groundwater. Thermodynamic data of GR_{SO4} and GR_{CO3} (Karimian et al., 2017; Drissi et al., 1995) were added to the MINTEQ database. Thermodynamically stable iron (oxyhydr)oxides (e.g., hematite, magnetite, goethite, lepidocrocite) were suppressed successively for calculations involving thermodynamically metastable Fe phases (Linke and Gislason, 2018). The reaction of HS^- and SO_4^{2-} was decoupled for speciation and solubility calculations for Fe and As species.

3. Results and discussion

3.1. Groundwater chemistry and predicted iron phases at the Collstrop site

The geochemical compositions of the three groundwaters collected at the CCA site are shown in Table S2. The As concentration was highest in the surface ditch water (~5000 μg L^{-1}, Eks.P1), and then clearly decreased with soil depth, as shown by As concentrations of ~134 μg L^{-1} in the shallow aquifer (129) and < 0.48 μg L^{-1} in the deep aquifer (MD2). These values fit well with measurements performed in 2009 (Aktor and Nielsen, 2011), and demonstrate that the highest degree of CCA contamination is still contained within the topmost soil layer, while As concentrations in the deep aquifer are below the threshold value set for water quality in Denmark (Ministry of Environment and Food of Denmark, 2017) of 5 μg L^{-1}. These new geochemical data (Table S2) were then used to calculate Eh-pH profiles (Fig. S1) to reaffirm the stability of GR phases in the anoxic zones and to discern potential GR transformation pathways.

The thermodynamic calculations revealed that under the prevalent anoxic conditions, GR phases (i.e., GR_{CO3}, GR_{SO4}) were stable (Eh-pH diagram shown in Fig. S1a). Specifically, under the circum-neutral, anoxic conditions characterizing well MD2 (the site, where the groundwater for the aging experiments was collected), GR_{SO4} was predicted to be the stable GR phase. Interestingly however, so far, only GR_{CO3} has been observed in these environments. For example, Christiansen et al. (2009a) documented the presence of GR_{CO3} in anoxic groundwater wells from another site in Denmark with a similar groundwater chemistry (i.e., circum-neutral pH, high concentrations of HCO_3^- and SO_4^{2-}). The dominance of GR_{CO3} over GR_{SO4} may be due to the abundance of CO_3^{2-} and its higher affinity for the GR interlayer compared to SO_4^{2-} (Refait et al., 1997). The calculations also confirmed that GR is thermodynamically metastable at circum-neutral to slightly basic pH and anoxic conditions and will eventually transform to more stable Fe (oxyhydr)oxides, in this case likely magnetite, as shown by the Eh-pH diagram after aging (Fig. S1b). Such transformations have been documented previously in laboratory experiments (Sumoondur et al., 2008).

3.2. GR stability in as-collected anoxic groundwater

Although GR_{SO4} phases should be stable in the sampled anoxic, circum-neutral pH groundwaters from a thermodynamic point of view, their long-term stabilities are not well known. Thus, we followed the changes in GR_{SO4} through aging experiments in the as-collected (i.e., As-free) anoxic groundwaters at 25 and 4 °C.

3.2.1. GR_{SO4} aging at 25 °C

The mineralogy of the solids changed from GR_{SO4} to GR_{CO3} (peak at ~11.8°, Fig. S2a) over the first 7 days of aging, with GR_{CO3} making up 80 % of the solids after 15 days. Trace amounts of magnetite could be detected (XRD peak at ~35.6°, Fig. S2a) after 15 days and this magnetite fraction increased at the expense of both GR_{SO4} and GR_{CO3}. After 120 days, magnetite was the dominant mineral phase (> 99 %), with only traces of GR left (Fig. 2a). In addition to GR phases and magnetite, trace amounts of another carbonate-intercalated layered double hydroxide (LDH) phase were detected in samples collected between day 7 and day 30 (Fig. S3a), indicating the presence of either a Mg(II)-Fe(III) LDH, also known as pyroaurite (Ingram and Taylor, 1967), or a partially Mg(II)-substituted GR_{CO3} (Refait et al., 2002). This GR to magnetite transformation documented by the XRD results was corroborated by SEM images that revealed thin hexagonal GR plates after 1 day (Fig. 2d), which were replaced by small isometric magnetite crystals in the 120 day sample (Fig. 2e). These mineral transformations were also mirrored in the changes in the associated solution chemistry. Specifically, a rapid increase in aqueous [Fe^{2+}] (Fig. 2b) coincided with the transformation of GR_{SO4} to GR_{CO3} between day 1 and day 15 (Fig. 2a). This suggests that GR_{SO4} partially dissolved during its transformation to GR_{CO3}. After 15 days, aqueous [Fe^{2+}] started to decrease, in conjunction with the gradual formation of magnetite and the disappearance of GR_{CO3}.

Interestingly among the other aqueous ions analyzed as a function of aging time, silica also changed during these GR transformations. Specifically, within 1 day, half of all initial dissolved silica ($[Si]_{initial}$ = ~16 mg L^{-1}) was removed, and almost all was removed by 30 days (Fig. 2c). At this time point GR phases still dominated, but during the GR to magnetite transformation Si was to a small extent re-released once GR started to transform to magnetite. The strong sorption behavior between Si and GR is in line with previous observations (Kwon et al., 2007; Yin et al., 2018). However, the rapid decrease in dissolved silica caused by the formation of a hydrated disordered Fe(II)-silicate "gel" (Tosca et al., 2016) cannot be completely ruled out.

3.2.2. GR_{SO4} aging at 4 °C

Similar mineralogical changes were observed when GR was aged at 4 °C. Compared to 25 °C, the changes occurred however, at much lower rates. For example, the initial GR_{SO4} significantly transformed to GR_{CO3} (~65 % conversion) only after 60 days, and only minor magnetite appeared after 120 days of reaction at 4 °C (Fig. 3a). Meanwhile, at 25

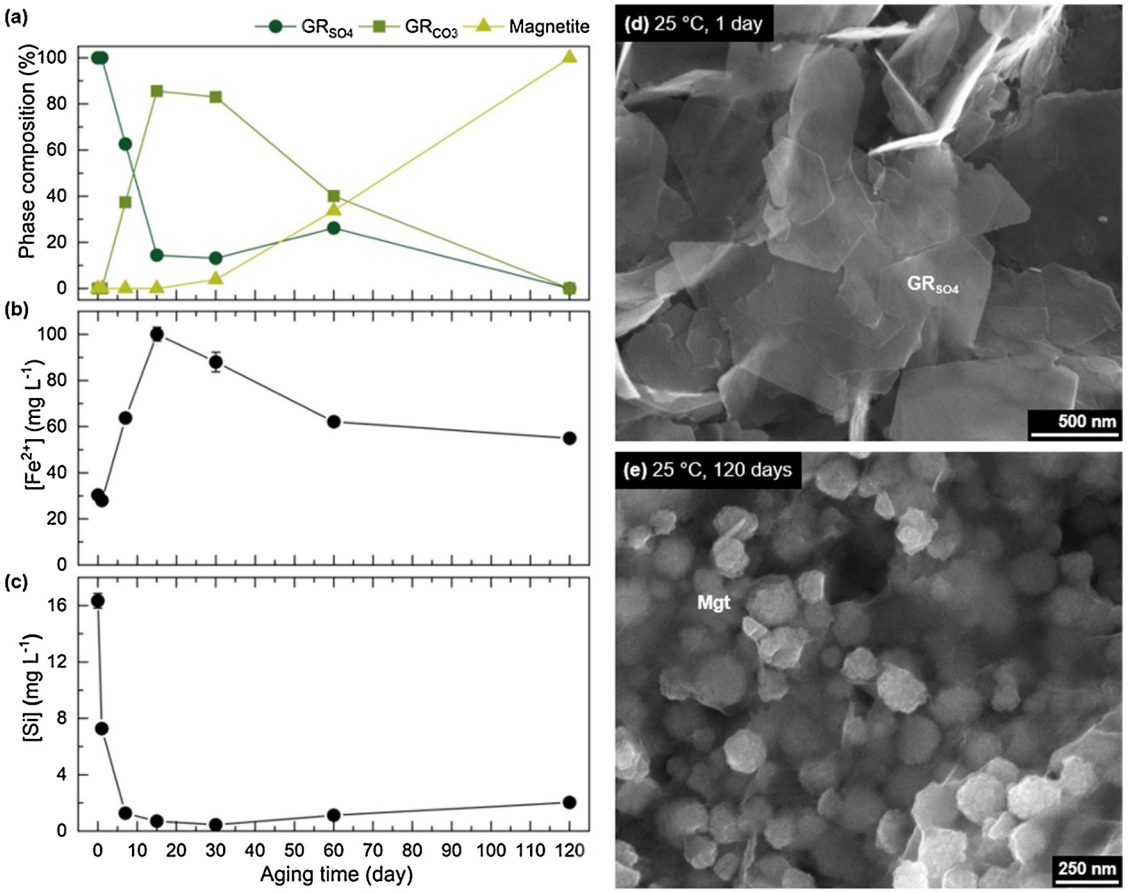

Fig. 2. Time evolution of the (a) solid phase mineralogy, (b) dissolved [Fe^{2+}] and (c) dissolved [Si] during aging of GR_{SO4} in anoxic groundwater at 25 °C over a period of 120 days. SEM image of solids collected after aging GR_{SO4} for (d) 1 day (thin hexagonal µm-sized GR_{SO4} platelets) and (e) 120 days (aggregates of magnetite nanoparticles). Considering that aqueous Fe^{3+} has a very low solubility (calculated maximum dissolved [Fe^{3+}] at circum-neutral pH = 10^{-12} mg L^{-1}) and can be assumed negligible (Cornell and Schwertmann, 2003). Thus, all measured dissolved iron in our aging experiments was present as [Fe^{2+}] (Perez et al., 2019b).

°C, GR_{CO3} and magnetite appeared already after 7 and 15 days, respectively. At the end of 120 days of aging at 4 °C, GR_{CO3} (~65 %) and GR_{SO4} (~34 %) were still the dominant phases (Fig. 3a), with magnetite constituting < 1 %. The presence of magnetite was documented primarily in SEM images where small isometric crystals appeared beside the hexagonal GR plates (Fig. 3e). Similar to reactions at 25 °C, the dissolved [Fe^{2+}] increased concomitantly with the formation of GR_{CO3} in the system (Fig. 3c), confirming that the interlayer exchange of sulfate with carbonate co-occurred with the partial dissolution of the GR_{SO4}. Again, similar to the 25 °C reaction, all dissolved Si was removed from solution by the present GR phases. However, Si re-release did not occur at 4 °C after 120 days, because magnetite formation was insignificant over this time frame.

Overall, these results showed that GR_{SO4} was indeed metastable and changed into GR_{CO3}, and eventually to magnetite as predicted by the thermodynamic calculations (Eh-pH diagrams, Fig. S1). However, temperature had a strong impact on the time scale of these transformations, indicating at least a 7-fold increase in GR_{SO4} long-term stability, with respect to GR_{SO4} transformation (see Table S3), by lowering the temperature from 25 to 4 °C. The observed trend of decreasing Si concentration with time in the reacting solutions is noteworthy, because it has been shown that sorbed Si inhibits GR transformation to other Fe (oxyhydr)oxides (Kwon et al., 2007).

3.3. GR aging in As-spiked anoxic groundwater

To assess the fate of potential As contamination in the deeper, anoxic aquifers, and to evaluate if its presence would impact the long-term stability of GR, we set-up similar GR_{SO4} aging experiments as above (both at 25 and 4 °C) but spiked the experimental reactors with a equimolar mixture of As(III) and As(V) (initial [As_{total}] = 6 mg L^{-1}).

3.3.1. GR_{SO4} aging at 25 °C with As

The results revealed that, at 25 °C, the presence of As prolonged the GR_{SO4} stability with significant GR_{CO3} only forming between day 60 and 120 (Fig. 4a), and trace amounts of magnetite (< 1 %) appearing after 120 days (again only documented through SEM images, Fig. 4b). Noteworthy is that, similar to As-free samples aged at 25 °C, a clear peak splitting of the ~11.8° peak of the GR_{CO3} could also be observed (Fig. S3b), which can be attributed to pyroaurite-like phases as discussed before (section 3.2.1; Ingram and Taylor, 1967; Refait et al., 2002). The addition of As in the groundwater increased the stability of GR_{SO4} by 8 times compared to GR_{SO4} aged in As-free groundwater at 25 °C (Table S3). Dissolved [Fe^{2+}] and dissolved [Si] mirror these trends as observed and discussed before (section 3.2). In terms of the behavior of the added aqueous As, our data showed that ~36 % of it was removed within the first day of aging, while the remainder was removed slowly but steadily, and almost all dissolved As was removed after 120 days aging. Comparing these trends (Fig. 4) to the As-free aging of GR_{SO4} (Fig. 2), it is clear that the added As temporarily stabilizes GR_{SO4}, delaying its transformation to GR_{CO3} and ultimately magnetite. This observed GR_{SO4} stabilization is best explained by fast adsorption of As species onto the initial GR_{SO4} particle surfaces as supported by the ~36 % removal of dissolved As, and the fact that all other parameters were identical between the As-spiked and As-free systems.

Such stabilization of the GR_{SO4} through the presence of As is

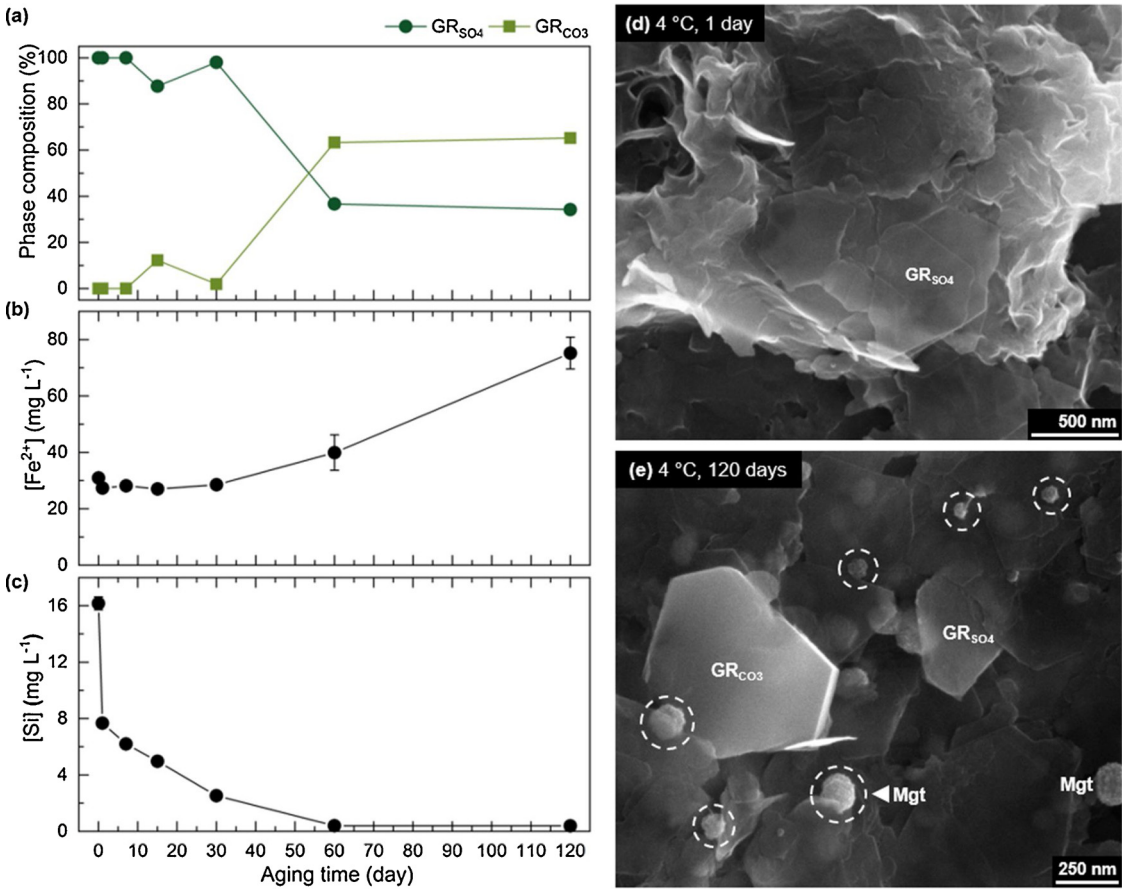

Fig. 3. Time evolution of the **(a)** solid phase mineralogy, **(b)** dissolved [Fe^{2+}] and **(c)** dissolved [Si] concentrations during aging of GR_{SO4} in anoxic groundwater at 4 °C over a period of 120 days. Corresponding SEM image of solids collected after aging GR_{SO4} for **(d)** 1 day (thin hexagonal µm-sized GR_{SO4} platelets) and **(e)** 120 days (mostly GR_{SO4} and thick hexagonal µm-sized GR_{CO3}, with small amounts of magnetite).

however surprising, considering that it took 120 days for As to be completely removed. For example, As adsorption by GR_{SO4} in ultrapure water systems at 25 °C and at similar As/Fe loadings is completed within 4 h (Perez et al., 2019a). The slower adsorption kinetics in groundwater observed here compared to the pure system probed by Perez et al. can partly be explained by the presence of other solutes with similarly high sorption affinities for GR. A primary sorption competitor in the water here is dissolved silica, seeing that it is abundant and structurally analogous to As, meaning it competes for the same GR surface sites as As (Kwon et al., 2007). In a previous study, it was shown that As sorption capacity by Fe (oxyhydr)oxides was reduced by up to ~70 % in the presence of 10 mg L^{-1} dissolved Si (Meng et al., 2000). Here, we see signs for this site competition as well. Specifically, we observed that the rate of Si removal is ~5 times slower in the As-spiked system compared to the As-free system (Table S4), indicating that Si is indeed competing with As for adsorption sites when they co-exist.

In addition, other common groundwater ions can also impact the sorption affinity of As onto GR surfaces. For example, the relatively high bicarbonate concentrations (~276 mg L^{-1} HCO_3^-) that were present in the collected groundwater might have further decreased As removal efficiencies through competitive sorption on GR as previously observed (Anawar et al., 2004; Stachowicz et al., 2007). Moreover, dissolved organic matter (~2 mg L^{-1} DOC) has been shown to form aqueous complexes with dissolved As, which can reduce is affinity for GR surface sites, or directly compete for GR sorption sites (Mladenov et al., 2015). Meanwhile, other potential sorption competitors including magnesium (Mg^{2+}) and phosphate (PO_4^{3-}) were also present. However, their concentrations were too low (Table S2) to have an impact on As removal here (Perez et al., 2019a). While we mainly attribute the slow As uptake rate to the presence of competing groundwater ions, it is also worth considering that we did not shake our reactor vessels during aging (i.e., they were left static), while those reported in Perez et al. (2019a) were continuously shaken. Thus, As-GR contact may have been hindered under these static conditions, which may also have contributed to lower As removal rates observed here.

3.3.2. GR_{SO4} aging at 4 °C with As

No significant changes in mineralogy were observed when GR_{SO4} was aged in As-spiked groundwater at 4 °C. GR_{SO4} was still the dominant mineral phase (~92 %) after 120 days and only a small amount of GR_{CO3} (~8 %) formed (Fig. 5a and b). This showed that the combined effects of added As and low temperature during aging increased the long-term GR_{SO4} stability by ~100 times compared to the As-free system at 25 °C (Table S3). The As removal rate was also much slower, with only ~66 % of the initial As immobilized after 120 days (Fig. 5d). This was also demonstrated by the calculated adsorption rate (Table S5), which is about 2 times lower at 4 °C than at 25 °C. Consequently, the trend of silica adsorption was very similar to As, with slower and incomplete removal (~86 %, Fig. 5e). These results indicate that low subsurface temperatures and the presence of adsorbed species significantly increase the long-term stability of GR_{SO4} in anoxic groundwater environments.

3.4. Mechanism of GR transformation and its implications on As mobility

The mobility and toxicity of arsenic in contaminated soils and groundwaters are often controlled by their interactions with mineral surfaces present in subsurface environments. Among such interactions,

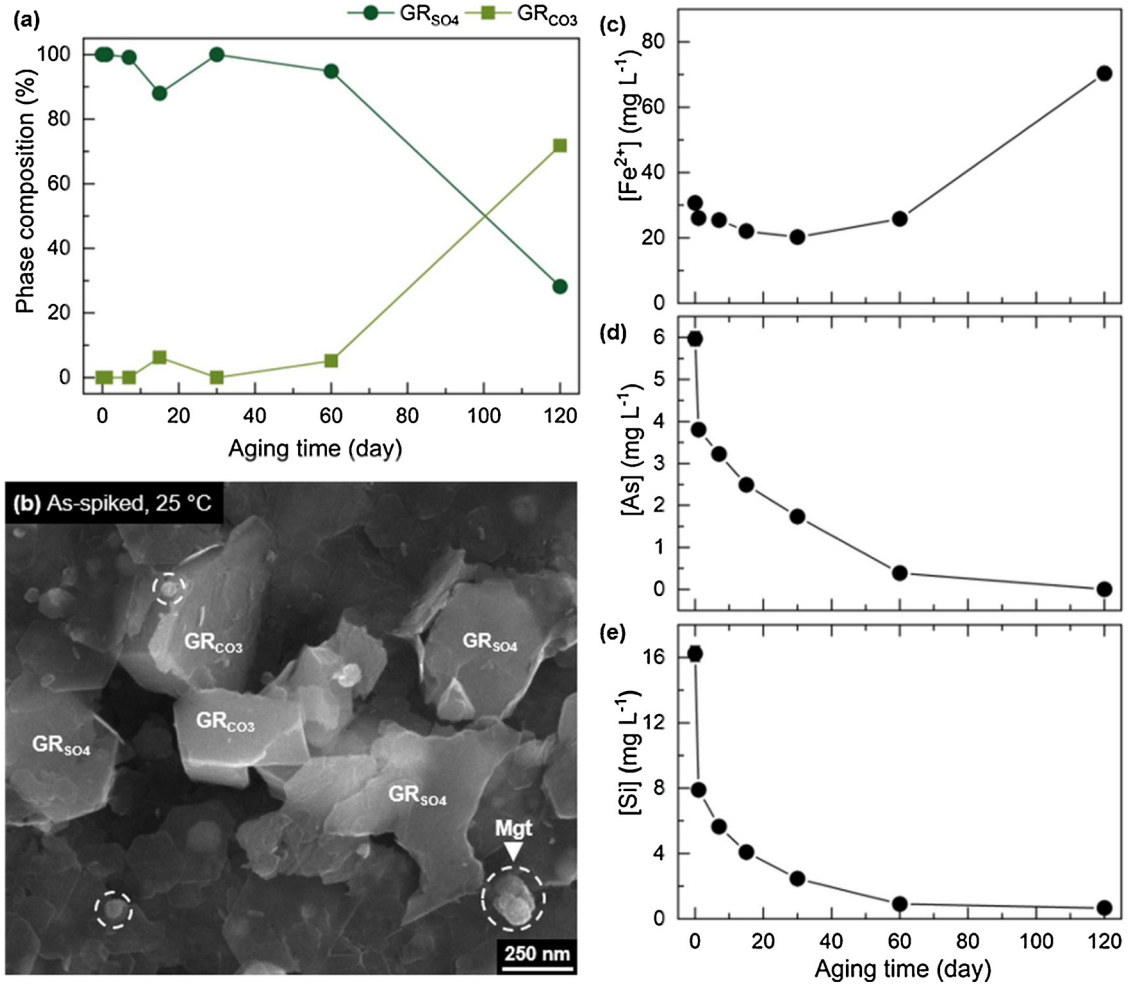

Fig. 4. (a) Time evolution of the solid phase mineralogy, with the **(b)** SEM image of the 120 days aged GR_{SO4} solids (showing partial transformation to GR_{CO3} and minor amounts of magnetite), and **(c)** dissolved [Fe^{2+}], **(d)** dissolved [As] and **(e)** dissolved [Si] during aging of GR_{SO4} in anoxic groundwater at 25 °C over a period of 120 days.

sorption affinity is one of the crucial parameters in controlling contaminant mobility. Naturally occurring iron (oxyhydr)oxides are very effective As sorbents and, specifically in ferruginous subsurface environments, GR phases most often form first (Christiansen et al., 2009a; Linke and Gislason, 2018) and effectively sequester toxic metals (Bearcock et al., 2011; Johnson et al., 2015) and metalloids (O'Loughlin et al., 2003; Perez et al., 2019a; Thomas et al., 2018). However, GR is a metastable phase in comparison to more thermodynamically stable iron (oxyhydr)oxides such as goethite or magnetite and often transform to these minerals with time (Sumoondur et al., 2008; Usman et al., 2018). Arsenic sequestered by GR phases may therefore be potentially remobilized and redistributed in the environment during such mineral transformations.

Our results showed that aging of synthetic GR_{SO4} at 25 °C in pristine (i.e., As-free) groundwater conditions first led to its partial conversion to GR_{CO3} within a few days, which was followed by gradual transformation of the GR phases to magnetite after 15 days. Full conversion to magnetite was seen after 120 days. Some trace Fe(III) oxyhydroxides (e.g., lepidocrocite and goethite) eventually appeared after 1 year, a reaction that has been documented before at low dissolved [Fe^{2+}] (< 2 mM) (Hansel et al., 2005; Pedersen et al., 2005). Comparing these results to GR_{SO4} aging experiments in ultrapure water showed that magnetite formation from GR was much slower in the natural groundwater matrix tested here compared to ultrapure water, where the same transformation took a few hours to maximum a few days (Ahmed et al., 2010; Sumoondur et al., 2008). We explain this enhanced GR stability by the presence of ions such as Si that can sorb to GR surfaces and prevent its dissolution and/or transformation (Kwon et al., 2007).

Aging of synthetic GR_{SO4} at 4 °C in pristine groundwater conditions led to much slower transformation rates compared to ambient conditions. GR_{SO4} only started transforming to GR_{CO3} after 60 days, and trace amounts of magnetite only appeared after 120 days. Even after one year of aging, the relative proportions of these phases did not change significantly (Fig. 6). This clearly indicates that low temperatures stabilize GR phases in subsurface environments. The increased stability of GR_{SO4} at low aging temperature is explained by iron (oxyhydr)oxides having lower solubilities at lower temperatures (Cornell and Schwertmann, 2003), meaning GR_{SO4} transformation rates to other iron (oxyhydr) oxides (i.e., GR_{CO3} and/or magnetite) are also lower. The strong influence of temperature on iron mineral transformations has also been observed for other iron (oxyhydr)oxides (Das et al., 2011; Schwertmann et al., 2004; Yee et al., 2006).

When synthetic GR_{SO4} was aged in As-spiked groundwater at 25 °C, the transformation to GR_{CO3} and magnetite were both delayed to 120 days, compared to the As-free system. Only further aging of the sample up to a year did ultimately result in magnetite formation (Fig. 6). We have shown in our recent work (Perez et al., 2020) that As(III) and As (V) form inner-sphere surface complexes at GR particle edges, and this is also well supported by previous studies (van Genuchten et al., 2019; Wang et al., 2010). Such surface complexes can prevent GR transformation by stabilizing the particle edges, thus inhibiting GR crystal

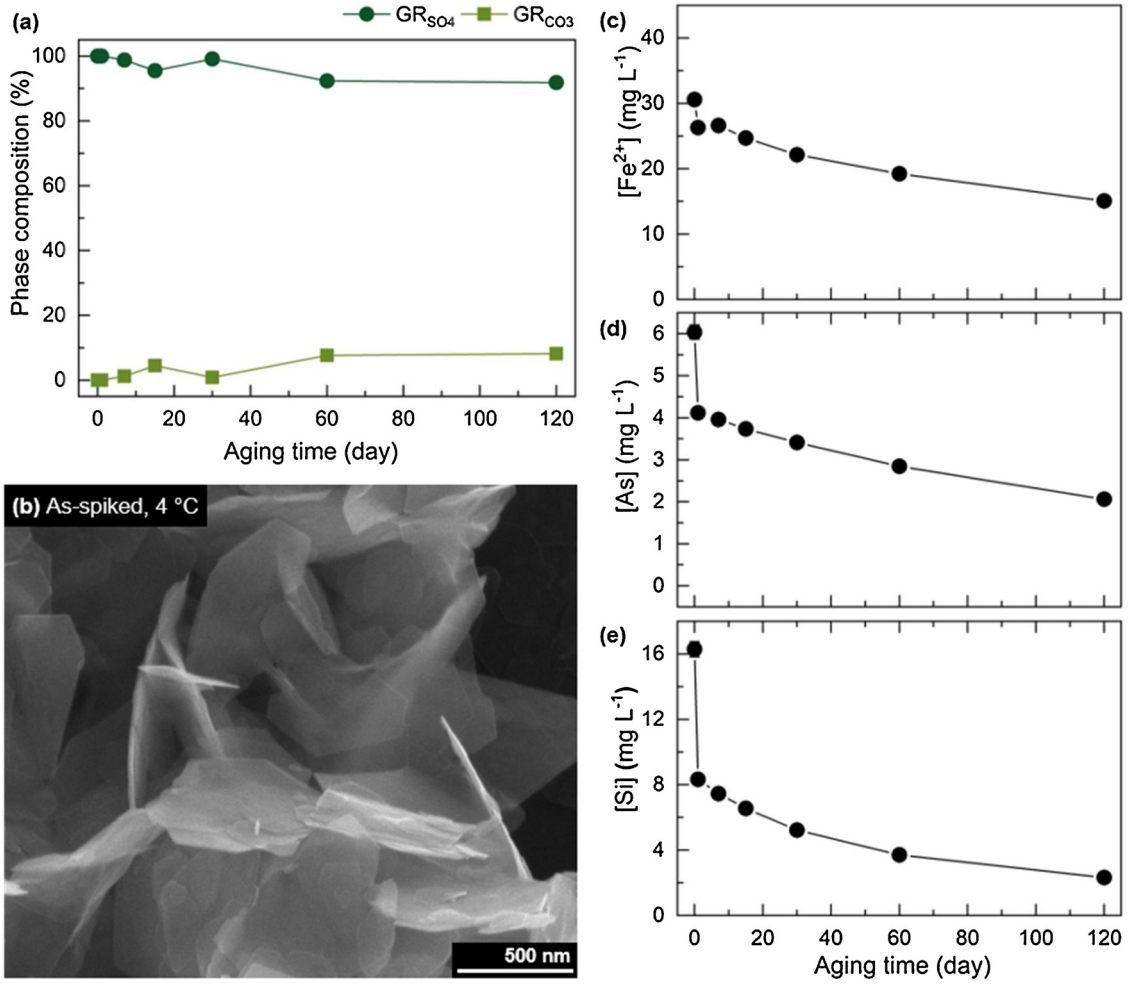

Fig. 5. **(a)** Time evolution of the solid phase mineralogy, with the **(b)** SEM image of the 120 days aged GR_{SO4} solids, and **(c)** dissolved [Fe^{2+}], **(d)** dissolved [As] and **(e)** dissolved [Si] during aging of GR_{SO4} in anoxic groundwater at 4 °C over a period of 120 days.

dissolution and precipitation of magnetite. Depending on the As oxidation state and amount of adsorbed As, magnetite formation can be delayed from days to a year (van Genuchten et al., 2019; Wang et al., 2014). Note that As(III) and/or As(V) intercalation in the GR structure is unlikely given that the XRD basal plane d-spacings for GR_{SO4} (001) and GR_{CO3} (003) were unchanged. Intercalation of As would have led to shifts in basal plane (00*l*) peak positions because the charge and, importantly, the ionic radii of AsO_3^{3-} (2.11 Å) and AsO_4^{3-} (2.48 Å) are different to that of SO_4^{2-} (2.30 Å) and CO_3^{2-} (1.89 Å) (Goh et al., 2008). Also, As intercalation was not observed in previous studies on As-GR interactions (Perez et al., 2020; van Genuchten et al., 2019;

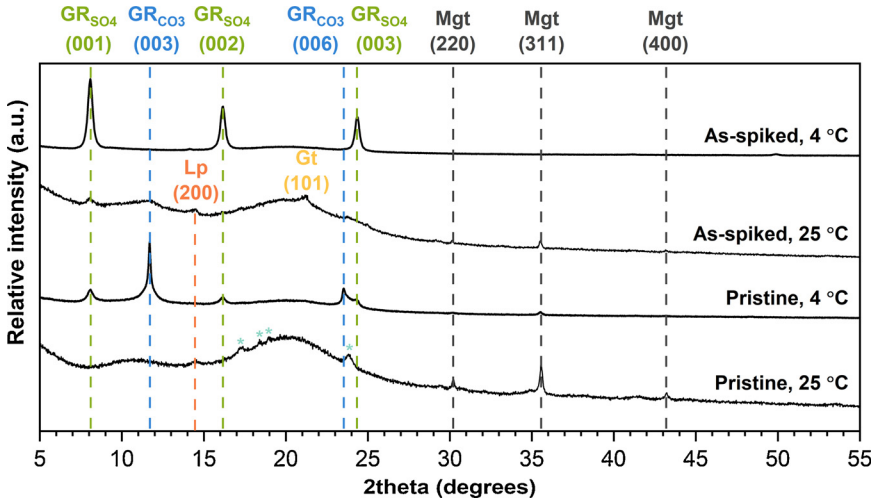

Fig. 6. XRD patterns showing the mineralogical composition of GR_{SO4} after aging for 1 year. Mgt, Lp and Gt denote magnetite, lepidocrocite and goethite, respectively. The peaks marked with '*' (light blue) in the pristine sample aged at 25 °C can be assigned to melanterite ($Fe^{II}SO_4$).

Wang et al., 2010).

An observation to further discuss is the observed Fe^{2+} release into solution during GR_{SO4} to GR_{CO3} transformations in this study. We explain this by GR_{SO4} and GR_{CO3} having different crystal structures, meaning transformation requires re-structuring. Specifically, GR_{CO3} has a rhombohedral lattice ($R\bar{3}m$ space group) with a stacking sequence of *AcBiBaCjCbA*… where *A*, *B* and *C* are the OH- layers, *a*, *b* and *c* are Fe (II)-Fe(III) cation layers and *i*, *j* and *k* are interlayer anions (Génin and Ruby, 2004; Refait et al., 1998). This stacking arrangement induces a three-layer repeat with a single plane of hydrated CO_3^{2-} anions. Meanwhile, GR_{SO4} has a trigonal lattice ($P\bar{3}m1$ space group) with a stacking sequence of *AcBij*…, resulting in a double-layer repeat with two planes of hydrated SO_4^{2-} anions (Christiansen et al., 2009b; Génin and Ruby, 2004; Simon et al., 2003). We hypothesize two possible transformation scenarios: (i) GR_{SO4} partially dissolves to enable interlayer exchange between SO_4^{2-} and CO_3^{2-}, and restructuring to the GR_{CO3} crystal lattice; and (ii) GR_{SO4} particles dissolve and re-precipitate as newly formed GR_{CO3} particles while interlayer exchange is not a governing mechanism. The latter scenario seems unlikely however, given that the reported GR_{CO3} solubility constant (log K = 39.1) is higher than that of GR_{SO4} (log K = 3.9) (Drissi et al., 1995; Refait et al., 1999; Rickard and Luther, 2007), i.e., GR_{CO3} is more soluble than GR_{SO4}. Therefore, we propose that the observed GR_{SO4} to GR_{CO3} transformation occurs via interlayer exchange, accompanied by partial GR_{SO4} dissolution to allow crystal lattice re-structuring.

In our experiments with natural groundwaters spiked with As at 25 °C, all As was ultimately removed from solution, despite the complex composition of the natural groundwater and the high concentration of competing ions such as dissolved silica and bicarbonate (Roberts et al., 2004; Zhang et al., 2017). Most importantly, the transformation of GR to magnetite did not result in any release of adsorbed As species into the supernatant. This is because magnetite can also effectively remove As either through surface adsorption (van Genuchten et al., 2020; Yean et al., 2005) or through incorporation in its crystal structure (Huhmann et al., 2017; van Genuchten et al., 2019).

At 4 °C, aging in As-spiked groundwater did not result in GR_{SO4} to GR_{CO3} transformation, showing the synergistic stabilizing effects of added As and low temperature. More than 90 % of the initial GR_{SO4} remained stable and no magnetite was detected even after aging for up to a year (Fig. 6). Our results were consistent with our thermodynamic calculations, which suggested that GR_{SO4} would indeed be the most stable Fe-bearing phase at the circum-neutral, anoxic conditions in our systems (Fig. S1). Our results at low temperature are particularly important because the temperature in the subsurface typically reflects the average annual air temperature at the surface with only a minor seasonal variation (Wisotzky et al., 2018). Previously measured temperatures in the deep wells at the Collstrop site are typically lower than 10 °C (Aktor and Nielsen, 2011), whereas average annual air temperature in Denmark is around 8.7 °C (Cappelen, 2012). The observed As removal rate was slower at subsurface temperatures (~66 % removal after 120 days), but complete removal (> 99 %) was achieved after one year of aging. Hence, it is likely that GR can efficiently remove As species in case of potential leakage into these subsurface environments, where low temperature significantly increases its long-term stability.

Overall, the increased stability of As-bearing GR_{SO4} (> 1 year) at low temperatures observed in this study gives important insights into how GR phases could help limit As mobility in the subsurface. Worth considering is also that biogeochemical processes in soils and sediments are dynamic; thus, GR formation and transformation processes will likely occur simultaneously and in close proximity in these anoxic subsurface environments. This means that GR phases will always be present if conditions favor its formation. This is supported by the fact that natural GR phases are observed in these environments (Christiansen et al., 2009a). Also, even if GR eventually transforms to magnetite (likely at time spans > 1 year), we do not expect any significant As release, given that magnetite has also been shown as an excellent scavenger for As here and in previous studies (van Genuchten et al., 2019, 2020).

Another point to consider here is that our experiments to a large extent excluded microbially-driven processes since groundwaters were filtered (0.2 μm) prior to testing. However, in these anoxic settings, iron reduction and oxidation reactions are in parts mediated by microbial processes (Melton et al., 2014), and microbial metabolism would therefore likely also influence GR formation and transformation processes. Several studies have reported the formation of GR phases during the bioreduction of Fe(III) (oxyhydr)oxides (e.g., ferrihydrite, lepidocrocite) by dissimilatory iron-reducing bacteria (DIRB) such as *Shewanella sp.* (O'Loughlin et al., 2007; Ona-Nguema et al., 2002; Zegeye et al., 2005). DIRB can also impact the toxicity and mobility of As; for example, *Shewanella sp.* can utilize both the Fe(III) in lepidocrocite and As(V) (aqueous and adsorbed species) as electron acceptors (Ona-Nguema et al., 2009). While the mineral-bound As(V) was completely reduced to As(III) during lepidocrocite bioreduction, no As release to solution was observed because the generated As(III) was sequestered in the resulting Fe(II)-bearing minerals (e.g., GR_{CO3}, Fe hydroxycarbonate, $Fe(OH)_2$). Some sulfate-reducing bacteria (SRB) such as *Desulfovibrio alaskensis* can also utilize biogenic GR_{SO4} as an electron acceptor during anaerobic respiration (Zegeye et al., 2007), resulting in the formation of GR_{CO3}, vivianite and iron sulfides. To our knowledge, there are no reported studies investigating the impact of SRB on the stability of As-bearing GR solids under anaerobic conditions. However, we suspect that As remobilization would still not occur under these conditions because As can be incorporated in the crystal structure of vivianite (Muehe et al., 2016), sorbed onto iron sulfides (Couture et al., 2013; Farquhar et al., 2002), or precipitated as amorphous or crystalline arsenic sulfides (Johnston et al., 2012; Kocar et al., 2010).

4. Conclusion

In this study, we examined the potential of GR for the natural attenuation of arsenic using natural groundwater from a former wood preservation site. Thermodynamic calculations based on the water chemistry of collected samples from the contaminated site showed that GR can form in these anoxic subsurface environments. We performed long-term batch experiments by aging synthetic GR_{SO4} in anoxic groundwater, with or without added As, at ambient (25 °C) and low (4 °C) temperatures. Arsenic was completely removed (> 99 %) from the natural groundwater after 120 days of aging at ambient temperatures, while the As removal rate was lower at lower temperature and complete removal was only achieved after one year of aging. The stability of GR_{SO4} during aging in natural groundwater was greatly affected by temperature and the presence of adsorbed As species. Under ambient temperature, GR_{SO4} transformed to GR_{CO3} and ultimately to magnetite within one month of aging in pristine groundwater. The addition of As to the groundwater significantly slowed down these mineral transformation rates due to the adsorption of As onto GR_{SO4}. A similar stabilization effect was achieved when GR_{SO4} was aged in pristine groundwater at 4 °C. Remarkably, GR_{SO4} remained stable for even up to one year when aged in As-spiked groundwater at 4 °C. Overall, our results highlight the importance of GR in removing As species from groundwater, and their potential as critical host phases for As in natural attenuation processes in contaminated subsurface environments.

CRediT authorship contribution statement

Jeffrey Paulo H. Perez: Conceptualization, Methodology, Investigation, Writing - original draft. **Adrian Alexander Schiefler:** Investigation, Writing - review & editing. **Sandra Navaz Rubio:** Formal analysis, Writing - review & editing. **Markus Reischer:** Resources, Writing - review & editing. **Niels Døssing Overheu:** Resources, Writing - review & editing. **Liane G. Benning:** Supervision, Funding acquisition, Writing - review & editing. **Dominique J. Tobler:** Supervision,

Funding acquisition, Project administration, Writing - review & editing.

Declaration of Competing Interest

The authors declare that they have no known competing financial interests or personal relationships that could have appeared to influence the work reported in this paper.

Acknowledgements

This project has received funding from the European Union's Horizon 2020 Marie Sklodowska-Curie Innovative Training Network Grant No. 675219. LGB acknowledges the financial support from the German Helmholtz Recruiting Initiative funding (award number I-044-16-01). All ICP-OES analyses were carried out at the Helmholtz Laboratory for the Geochemistry of the Earth Surface (HELGES) at GFZ Potsdam. The authors would like to thank Marco Mangayayam from University of Copenhagen for his help with GR synthesis, Stephen Reid from University of Leeds for ICP-MS analyses and Matthias Winkel from the Interface Geochemistry Section at GFZ for the help with IC analyses.

Appendix A. Supplementary data

Supplementary material related to this article can be found, in the online version, at doi:https://doi.org/10.1016/j.jhazmat.2020.123327.

References

Abdelmoula, M., Trolard, F., Bourrie, G., Genin, J.M.R., 1998. Evidence for the Fe(II)-Fe(III) Green Rust "Fougerite" mineral occurrence in a hydromorphic soil and its transformation with depth. Hyperfine Interact. 112, 235–238.

Ahmed, I.A., Benning, L.G., Kakonyi, G., Sumoondur, A.D., Terrill, N.J., Shaw, S., 2010. Formation of green rust sulfate: a combined in situ time-resolved X-ray scattering and electrochemical study. Langmuir 26, 6593–6603.

Aktor, H., Nielsen, K.A., 2011. Investigation and Risk Assessment of Collstrop Site in Relation to Esrum Lake (in Danish). Danish Environmental Proctection Agency, Copenhagen, Denmark.

Anawar, H.M., Akai, J., Sakugawa, H., 2004. Mobilization of arsenic from subsurface sediments by effect of bicarbonate ions in groundwater. Chemosphere 54, 753–762.

Asta, M.P., Ayora, C., Roman-Ross, G., Cama, J., Acero, P., Gault, A.G., Charnock, J.M., Bardelli, F., 2010. Natural attenuation of arsenic in the Tinto Santa Rosa acid stream (Iberian Pyritic Belt, SW Spain): the role of iron precipitates. Chem. Geol. 271, 1–12.

Bearcock, J.M., Perkins, W.T., Dinelli, E., Wade, S.C., 2006. Fe(II)/Fe(III)' green rust' developed within ochreous coal mine drainage sediment in South Wales, UK. Mineral. Mag. 70, 731–741.

Bearcock, J.M., Perkins, W.T., Pearce, N.J., 2011. Laboratory studies using naturally occurring "green rust" to aid metal mine water remediation. J. Hazard. Mater. 190, 466–473.

Bethke, C.M., 2010. Geochemical and Biogeochemical Reaction Modeling. Cambridge University Press.

Bhattacharya, P., Mukherjee, A.B., Jacks, G., Nordqvist, S., 2002. Metal contamination at a wood preservation site: characterisation and experimental studies on remediation. Sci. Total Environ. 290, 165–180.

Cappelen, J., 2012. Denmark - DMI Historical Climate Data Collection 1768-2011 Technical Report 12-02. Danish Meteorological Institute pp. 90.

Carlson, L., Bigham, J.M., Schwertmann, U., Kyek, A., Wagner, F., 2002. Scavenging of As from acid mine drainage by schwertmannite and ferrihydrite: a comparison with synthetic analogues. Environ. Sci. Technol. 36, 1712–1719.

Christiansen, B.C., Balic-Zunic, T., Dideriksen, K., Stipp, S.L., 2009a. Identification of green rust in groundwater. Environ. Sci. Technol. 43, 3436–3441.

Christiansen, B.C., Balic-Zunic, T., Petit, P.O., Frandsen, C., Morup, S., Geckeis, H., Katerinopoulou, A., Stipp, S.L.S., 2009b. Composition and structure of an iron-bearing, layered double hydroxide (LDH) - Green rust sodium sulphate. Geochim. Cosmochim. Acta 73, 3579–3592.

Christiansen, B.C., Dideriksen, K., Katz, A., Nedel, S., Bovet, N., Sorensen, H.O., Frandsen, C., Gundlach, C., Andersson, M.P., Stipp, S.L., 2014. Incorporation of monovalent cations in sulfate green rust. Inorg. Chem. 53, 8887–8894.

Cornell, R.M., Schwertmann, U., 2003. The Iron Oxides: Structure, Properties, Reactions, Occurrences and Uses. Wiley-VCH Verlag GmbH & Co. KGaA, Weinheim, FRG.

Couture, R.M., Rose, J., Kumar, N., Mitchell, K., Wallschläger, D., Van Cappellen, P., 2013. Sorption of arsenite, arsenate, and thioarsenates to iron oxides and iron sulfides: a kinetic and spectroscopic Investigation. Environ. Sci. Technol. 47, 5652–5659.

Das, S., Hendry, M.J., Essilfie-Dughan, J., 2011. Transformation of two-line ferrihydrite to goethite and hematite as a function of pH and temperature. Environ. Sci. Technol. 45, 268–275.

Dore, E., Fancello, D., Rigonat, N., Medas, D., Cidu, R., Da Pelo, S., Frau, F., Lattanzi, P., Marras, P.A., Meneghini, C., Podda, F., Rimondi, V., Runkel, R.L., Kimball, B., Wanty, R.B., De Giudici, G., 2020. Natural attenuation can lead to environmental resilience in mine environment. Appl. Geochem. 117, 104597.

Drissi, S.H., Refait, P., Abdelmoula, M., Genin, J.M.R., 1995. The Preparation and thermodynamic properties of Fe(II)-Fe(III) hydroxide-carbonate (Green-Rust-1) - Pourbaix diagram of iron in carbonate-containing aqueous-media. Corros. Sci. 37, 2025–2041.

Farquhar, M.L., Charnock, J.M., Livens, F.R., Vaughan, D.J., 2002. Mechanisms of arsenic uptake from aqueous solution by interaction with goethite, lepidocrocite, mackinawite, and pyrite: an X-ray absorption spectroscopy study. Environ. Sci. Technol. 36, 1757–1762.

Fukushi, K., Sasaki, M., Sato, T., Yanase, N., Amano, H., Ikeda, H., 2003. A natural attenuation of arsenic in drainage from an abandoned arsenic mine dump. Appl. Geochem. 18, 1267–1278.

Génin, J.-M.R., Ruby, C., 2004. Anion and cation distributions in Fe(II–III) hydroxysalt green rusts from XRD and Mössbauer analysis (carbonate, chloride, sulphate, …); the "fougerite" mineral. Solid State Sci. 6, 705–718.

Goh, K.H., Lim, T.T., Dong, Z., 2008. Application of layered double hydroxides for removal of oxyanions: a review. Water Res. 42, 1343–1368.

Hansel, C.M., Benner, S.G., Fendorf, S., 2005. Competing Fe (II)-induced mineralization pathways of ferrihydrite. Environ. Sci. Technol. 39, 7147–7153.

Hingston, J.A., Collins, C.D., Murphy, R.J., Lester, J.N., 2001. Leaching of chromated copper arsenate wood preservatives: a review. Environ. Pollut. 111, 53–66.

Huhmann, B.L., Neumann, A., Boyanov, M.I., Kemner, K.M., Scherer, M.M., 2017. Emerging investigator series: As(v) in magnetite: incorporation and redistribution. Environ. Sci. Process. Impacts 19, 1208–1219.

Humphrey, D.G., 2002. The chemistry of chromated copper arsenate wood preservatives. Rev. Inorg. Chem. 22, 1–40.

Ingram, L., Taylor, H.F.W., 1967. The crystal structures of sjögrenite and pyroaurite. Mineral. Mag. 36, 465–479.

Johnson, C.A., Freyer, G., Fabisch, M., Caraballo, M.A., Kusel, K., Hochella, M.F., 2014. Observations and assessment of iron oxide and green rust nanoparticles in metal-polluted mine drainage within a steep redox gradient. Environ. Chem. 11, 377–391.

Johnson, C.A., Murayama, M., Kusel, K., Hochella, M.F., 2015. Polycrystallinity of green rust minerals and their synthetic analogs: implications for particle formation and reactivity in complex systems. Am. Mineral. 100, 2091–2105.

Johnston, S.G., Burton, E.D., Keene, A.F., Planer-Friedrich, B., Voegelin, A., Blackford, M.G., Lumpkin, G.R., 2012. Arsenic mobilization and iron transformations during sulfidization of As(V)-bearing jarosite. Chem. Geol. 334, 9–24.

Karimian, N., Johnston, S.G., Burton, E.D., 2017. Antimony and arsenic behavior during Fe(II)-Induced transformation of jarosite. Environ. Sci. Technol. 51, 4259–4268.

Kocar, B.D., Borch, T., Fendorf, S., 2010. Arsenic repartitioning during biogenic sulfidization and transformation of ferrihydrite. Geochim. Cosmochim. Acta 74, 980–994.

Koeksoy, E., Sundman, A., Byrne, J.M., Lohmayer, R., Planer-Friedrich, B., Halevy, I., Konhauser, K.O., Kappler, A., 2019. Formation of green rust and elemental sulfur in an analogue for oxygenated ferro-euxinic transition zones of Precambrian oceans. Geology 47, 211–214.

Kwon, S.K., Kimijima, K., Kanie, K., Suzuki, S., Muramatsu, A., Saito, M., Shinoda, K., Waseda, Y., 2007. Influence of silicate ions on the formation of goethite from green rust in aqueous solution. Corros. Sci. 49, 2946–2961.

Linke, T., Gislason, S.R., 2018. Stability of iron minerals in Icelandic peat areas and transport of heavy metals and nutrients across oxidation and salinity gradients - a modelling approach. Carbon Nat. Eng. Process. 146, 30–37.

Maillot, F., Morin, G., Juillot, F., Bruneel, O., Casiot, C., Ona-Nguema, G., Wang, Y.H., Lebrun, S., Aubry, E., Vlaic, G., Brown, G.E., 2013. Structure and reactivity of As(III)- and As(V)-rich schwertmannites and amorphous ferric arsenate sulfate from the Carnoules acid mine drainage, France: comparison with biotic and abiotic model compounds and implications for As remediation. Geochim. Cosmochim. Acta 104, 310–329.

Mangayayam, M.C., Dideriksen, K., Tobler, D.J., 2018. Can or cannot green rust reduce chlorinated ethenes? Carbon Nat. Eng. Process. 146, 173–178.

Masscheleyn, P.H., Delaune, R.D., Patrick, W.H., 1991. Arsenic and selenium chemistry as affected by sediment redox potential and ph. J. Environ. Qual. 20, 522–527.

Melton, E.D., Swanner, E.D., Behrens, S., Schmidt, C., Kappler, A., 2014. The interplay of microbially mediated and abiotic reactions in the biogeochemical Fe cycle. Nat. Rev. Microbiol. 12, 797–808.

Meng, X.G., Bang, S., Korfiatis, G.P., 2000. Effects of silicate, sulfate, and carbonate on arsenic removal by ferric chloride. Water Res. 34, 1255–1261.

Ministry of Environment and Food of Denmark, 2017. Bekendtgørelse om vandkvalitet og tilsyn med vandforsyningsanlæg. BEK no. 1147 of 24/10/2017. .

Mladenov, N., Zheng, Y., Simone, B., Bilinski, T.M., McKnight, D.M., Nemergut, D., Radloff, K.A., Rahman, M.M., Ahmed, K.M., 2015. Dissolved organic matter quality in a shallow aquifer of Bangladesh: implications for arsenic mobility. Environ. Sci. Technol. 49, 10815–10824.

Muehe, E.M., Morin, G., Scheer, L., Pape, P.L., Esteve, I., Daus, B., Kappler, A., 2016. Arsenic(V) incorporation in vivianite during microbial reduction of arsenic(V)-bearing biogenic Fe(III) (oxyhydr)oxides. Environ. Sci. Technol. 50, 2281–2291.

Nielsen, S.S., Petersen, L.R., Kjeldsen, P., Jakobsen, R., 2011. Amendment of arsenic and chromium polluted soil from wood preservation by iron residues from water treatment. Chemosphere 84, 383–389.

Nielsen, S.S., Kjeldsen, P., Jakobsen, R., 2016. Full scale amendment of a contaminated wood impregnation site with iron water treatment residues. Front. Environ. Sci. Eng. 10, 3.

O'Loughlin, E.J., Kelly, S.D., Cook, R.E., Csencsits, R., Kemner, K.M., 2003. Reduction of uranium(VI) by mixed iron(II)/iron(III) hydroxide (green rust): formation of UO2 nanoparticles. Environ. Sci. Technol. 37, 721–727.

O'Loughlin, E.J., Larese-Casanova, P., Scherer, M., Cook, R., 2007. Green rust formation from the bioreduction of γ –FeOOH (Lepidocrocite): comparison of several Shewanella species. Geomicrobiol. J. 24, 211–230.
Ona-Nguema, G., Abdelmoula, M., Jorand, F., Benali, O., Gehin, A., Block, J.C., Genin, J.M., 2002. Iron(II,III) hydroxycarbonate green rust formation and stabilization from lepidocrocite bioreduction. Environ. Sci. Technol. 36, 16–20.
Ona-Nguema, G., Morin, G., Wang, Y.H., Menguy, N., Juillot, F., Olivi, L., Aquilanti, G., Abdelmoula, M., Ruby, C., Bargar, J.R., Guyot, F., Calas, G., Brown, G.E., 2009. Arsenite sequestration at the surface of nano-Fe(OH)(2), ferrous-carbonate hydroxide, and green-rust after bioreduction of arsenic-sorbed lepidocrocite by Shewanella putrefaciens. Geochim. Cosmochim. Acta 73, 1359–1381.
Pedersen, H.D., Postma, D., Jakobsen, R., Larsen, O., 2005. Fast transformation of iron oxyhydroxides by the catalytic action of aqueous Fe(II). Geochim. Cosmochim. Acta 69, 3967–3977.
Perez, J.P.H., Freeman, H.M., Schuessler, J.A., Benning, L.G., 2019a. The interfacial reactivity of arsenic species with green rust sulfate (GR_{SO4}). Sci. Total Environ. 648, 1161–1170.
Perez, J.P.H., Tobler, D.J., Thomas, A.N., Freeman, H.M., Dideriksen, K., Radnik, J., Benning, L.G., 2019b. Adsorption and reduction of arsenate during the Fe2+-Induced transformation of ferrihydrite. ACS Earth Space Chem. 3, 884–894.
Perez, J.P.H., Freeman, H.M., Brown, A.P., van Genuchten, C.M., Dideriksen, K., S'Ari, M., Tobler, D.J., Benning, L.G., 2020. Direct visualization of arsenic binding on green rust sulfate. Environ. Sci. Technol. 54, 3297–3305.
Raghav, M., Shan, J., Saez, A.E., Ela, W.P., 2013. Scoping candidate minerals for stabilization of arsenic-bearing solid residuals. J. Hazard. Mater. 263 Pt 2, 525–532.
Refait, P., Drissi, S.H., Pytkiewicz, J., Genin, J.M.R., 1997. The anionic species competition in iron aqueous corrosion: role of various green rust compounds. Corros. Sci. 39, 1699–1710.
Refait, P.H., Abdelmoula, M., Genin, J.M.R., 1998. Mechanisms of formation and structure of green rust one in aqueous corrosion of iron in the presence of chloride ions. Corros. Sci. 40, 1547–1560.
Refait, P., Bon, C., Simon, L., Bourrie, G., Trolard, F., Bessiere, J., Genin, J.M.R., 1999. Chemical composition and Gibbs standard free energy of formation of Fe(II)-Fe(III) hydroxysulphate green rust and Fe(II) hydroxide. Clay Miner. 34, 499–510.
Refait, P.H., Drissi, S., Abdelmoula, M., Genin, J.M.R., 2002. Synthesis and reactivity of Mg(II)-Fe(II)-Fe(III) hydroxycarbonates. Hyperfine Interact. 139, 651–655.
Reisinger, H.J., Burris, D.R., Hering, J.G., 2005. Remediating Subsurface Arsenic Contamination With Monitored Natural Attenuation. ACS Publications.
Rennert, T., Eusterhues, K., De Andrade, V., Totsche, K.U., 2012. Iron species in soils on a mofette site studied by Fe *K*-edge X-ray absorption near-edge spectroscopy. Chem. Geol. 332, 116–123.
Rickard, D., Luther 3rd, G.W., 2007. Chemistry of iron sulfides. Chem. Rev. 107, 514–562.
Roberts, L.C., Hug, S.J., Ruettimann, T., Billah, M., Khan, A.W., Rahman, M.T., 2004. Arsenic removal with iron(II) and iron(III) in waters with high silicate and phosphate concentrations. Environ. Sci. Technol. 38, 307–315.
Root, R.A., Dixit, S., Campbell, K.M., Jew, A.D., Hering, J.G., O'Day, P.A., 2007. Arsenic sequestration by sorption processes in high-iron sediments. Geochim. Cosmochim. Acta 71, 5782–5803.
Schwertmann, U., Stanjek, H., Becher, H.H., 2004. Long-term in vitro transformation of 2-line ferrihydrite to goethite/hematite at 4, 10, 15 and 25 degrees C. Clay Miner. 39, 433–438.
Simon, L., Francois, M., Refait, P., Renaudin, G., Lelaurain, M., Genin, J.M.R., 2003. Structure of the Fe(II-III) layered double hydroxysulphate green rust two from Rietveld analysis. Solid State Sci. 5, 327–334.
Stachowicz, M., Hiemstra, T., van Riemsdijk, W.H., 2007. Arsenic-bicarbonate interaction on goethite particles. Environ. Sci. Technol. 41, 5620–5625.
Stilwell, D.E., Gorny, K.D., 1997. Contamination of soil with copper, chromium, and arsenic under decks built from pressure treated wood. Bull. Environ. Contam. Toxicol. 58, 22–29.
Sumoondur, A., Shaw, S., Ahmed, I., Benning, L.G., 2008. Green rust as a precursor for magnetite: an in situ synchrotron based study. Mineral. Mag. 72, 201–204.
Thomas, A.N., Eiche, E., Göttlicher, J., Steininger, R., Benning, L.G., Freeman, H.M., Dideriksen, K., Neumann, T., 2018. Products of hexavalent chromium reduction by green rust sodium sulfate and associated reaction mechanisms. Soil Syst. 2, 58.
Toby, B.H., Von Dreele, R.B., 2013. GSAS-II: the genesis of a modern open-source all purpose crystallography software package. J. Appl. Crystallogr. 46, 544–549.
Tosca, N.J., Guggenheim, S., Pufahl, P.K., 2016. An authigenic origin for Precambrian greenalite: implications for iron formation and the chemistry of ancient seawater. Geol. Soc. Am. Bull. 128, 511–530.
Trolard, F., Genin, J.M.R., Abdelmoula, M., Bourrie, G., Humbert, B., Herbillon, A., 1997. Identification of a green rust mineral in a reductomorphic soil by Mossbauer and Raman spectroscopies. Geochim. Cosmochim. Acta 61, 1107–1111.
Usman, M., Byrne, J.M., Chaudhary, A., Orsetti, S., Hanna, K., Ruby, C., Kappler, A., Haderlein, S.B., 2018. Magnetite and green rust: synthesis, properties, and environmental applications of mixed-valent iron minerals. Chem. Rev. 118, 3251–3304.
van Genuchten, C.M., Behrends, T., Dideriksen, K., 2019. Emerging investigator series: interdependency of green rust transformation and the partitioning and binding mode of arsenic. Environ. Sci.: Process Impacts 21, 1459–1476.
van Genuchten, C.M., Behrends, T., Stipp, S.L.S., Dideriksen, K., 2020. Achieving arsenic concentrations of < 1 μg/L by Fe(0) electrolysis: the exceptional performance of magnetite. Water Res. 168, 115170.
Viollier, E., Inglett, P.W., Hunter, K., Roychoudhury, A.N., Van Cappellen, P., 2000. The ferrozine method revisited: Fe(II)/Fe(III) determination in natural waters. Appl. Geochem. 15, 785–790.
Vuillemin, A., Wirth, R., Kemnitz, H., Schleicher, A.M., Friese, A., Bauer, K.W., Simister, R., Nomosatryo, S., Ordonez, L., Ariztegui, D., Henny, C., Crowe, S.A., Benning, L.G., Kallmeyer, J., Russell, J.M., Bijaksana, S., Vogel, H., Team, T.D.P.S., 2019. Formation of diagenetic siderite in modern ferruginous sediments. Geology 47, 540–544.
Wang, S., Mulligan, C.N., 2006. Natural attenuation processes for remediation of arsenic contaminated soils and groundwater. J. Hazard. Mater. 138, 459–470.
Wang, Y., Morin, G., Ona-Nguema, G., Juillot, F., Guyot, F., Calas, G., Brown, G.E., 2010. Evidence for different surface speciation of arsenite and arsenate on green rust: an EXAFS and XANES study. Environ. Sci. Technol. 44, 109–115.
Wang, Y., Morin, G., Ona-Nguema, G., Brown Jr, G.E., 2014. Arsenic(III) and arsenic(V) speciation during transformation of lepidocrocite to magnetite. Environ. Sci. Technol. 48, 14282–14290.
Wisotzky, F., Cremer, N., Lenk, S., 2018. Angewandte Grundwasserchemie, Hydrogeologie Und Hydrogeochemische Modellierung: Grundlagen, Anwendungen Und Problemlösungen. Springer, Berlin Heidelberg.
Yean, S., Cong, L., Yavuz, C.T., Mayo, J.T., Yu, W.W., Kan, A.T., Colvin, V.L., Tomson, M.B., 2005. Effect of magnetite particle size on adsorption and desorption of arsenite and arsenate. J. Mater. Res. 20, 3255–3264.
Yee, N., Shaw, S., Benning, L.G., Nguyen, T.H., 2006. The rate of ferrihydrite transformation to goethite via the Fe(II) pathway. Am. Mineral. 91, 92–96.
Yin, W., Ai, J., Huang, L.Z., Tobler, D.J., HC, B.H., 2018. A Silicate/Glycine switch to control the reactivity of layered Iron(II)-Iron(III) hydroxides for dechlorination of Carbon Tetrachloride. Environ. Sci. Technol. 52, 7876–7883.
Zagury, G.J., Samson, R., Deschenes, L., 2003. Occurrence of metals in soil and ground water near chromated copper arsenate-treated utility poles. J. Environ. Qual. 32, 507–514.
Zagury, G.J., Dobran, S., Estrela, S., Deschenes, L., 2008. Inorganic arsenic speciation in soil and groundwater near in-service chromated copper arsenate-treated wood poles. Environ. Toxicol. Chem. 27, 799–807.
Zegeye, A., Ona-Nguema, G., Carteret, C., Huguet, L., Abdelmoula, M., Jorand, F., 2005. Formation of hydroxysulphate green rust 2 as a single iron(II-III) mineral in microbial culture. Geomicrobiol. J. 22, 389–399.
Zegeye, A., Huguet, L., Abdelmoula, M., Carteret, C., Mullet, M., Jorand, F., 2007. Biogenic hydroxysulfate green rust, a potential electron acceptor for SRB activity. Geochim. Cosmochim. Acta 71, 5450–5462.
Zegeye, A., Bonneville, S., Benning, L.G., Sturm, A., Fowle, D.A., Jones, C., Canfield, D.E., Ruby, C., MacLean, L.C., Nomosatryo, S., Crowe, S.A., Poulton, S.W., 2012. Green rust formation controls nutrient availability in a ferruginous water column. Geology 40, 599–602.
Zhang, D., Guo, H., Xiu, W., Ni, P., Zheng, H., Wei, C., 2017. In-situ mobilization and transformation of iron oxides-adsorbed arsenate in natural groundwater. J. Hazard. Mater. 321, 228–237.